Mon. Not. R. Astron. Soc. **000**, 1–19 (2010) Printed 17 May 2010 (MN LATEX style file v2.2)

A Census of Nuclear Stellar Disks in Early-type Galaxies

H. R. Ledo[1⋆], M. Sarzi[1], M. Dotti[2], S. Khochfar[3] and L. Morelli[4]
[1] *Centre for Astrophysics Research, University of Hertfordshire, College Lane, Hatfield AL10 9AB, United Kingdom*
[2] *Max-Planck-Institut für Astrophysik, Karl-Schwarzschild-Str. 1, D-85748 Garching, Germany*
[3] *Max-Planck-Institute für extraterrestrische Physik, Giessenbachstraβe, D-85748 Garching, Germany*
[4] *Dipartimento di Astronomia, Università di Padova, vicolo dell Osservatorio 2, 35122 Padova, Italy*

17 May 2010

ABSTRACT
Nuclear Stellar Disks (NSDs), of a few tens to hundreds of parsec across, are a common and yet poorly studied feature of early-type galaxies. Still, such small disks represent a powerful tool to constrain the assembling history of galaxies, since they can be used to trace to the epoch when galaxies experienced their last major merger event. By studying the fraction and stellar age of NSDs it is thus possible to test the predictions for the assembly history of early-type galaxies according the current hierarchical paradigm for galaxy formation. In this paper we have produced the most comprehensive census of NSDs in nearby early-type galaxies by searching for such disks in objects within 100 Mpc and by using archival images from the Hubble Space Telescope. We found that NSDs are present in approximately 20% of early-type galaxies, and that the fraction of galaxies with NSDs does not depend on their Hubble type nor on their galactic environment, whereas the incidence of NSDs appears to decline in the most massive systems. Furthermore, we have separated the light contribution of twelve such disks from that of their surrounding stellar bulge in order to extract their physical properties. This doubles the number of decomposed NSDs and although the derived values for their central surface brightness and scale-length are consistent with previous studies they also give a hint of possible different characteristics due to different formation scenario between nuclear disks and other kinds of large galactic disks.

Key words: galaxies: elliptical and lenticular, cD – galaxies: evolution

1 INTRODUCTION

More than a decade ago, Hubble Space Telescope (HST) observations revealed the presence of Nuclear Stellar Disks in several galaxies (van den Bosch *et al.* 1994a). These disks are distinct nuclear components with a few tens to hundreds of parsecs in diameter and have since then been recognised as a relatively common feature in early-type galaxies (e.g. Rest *et al.* 2001) while being notably rare in spirals (Pizzella *et al.* 2002). Despite the relatively high frequency of NSDs only a few studies were aimed at deriving their fundamental properties (Morelli *et al.* 2004; Pizzella *et al.* 2002; Scorza and van den Bosch 1998a), whereas the interest in NSD revolved mainly around their dynamically cold character, which facilitates the mass measurement of central supermassive black holes (SMBHs) (e.g., van den Bosch and de Zeeuw 1996).

Yet, NSDs may constitute a unique tool to constrain the assembling history of galaxies. NSDs are indeed fragile structures that should not survive a major merger event involving their host galaxy, which makes them useful clocks to trace the epoch since such an event occurred. Simple N-body simulations serve to illustrate the delicate nature of NSDs (Fig. 1). Following Dotti *et al.* (2007) we set up a stable stellar disk that is 200 pc across, $10^8 M_\odot$ in mass and which is orbiting around a central SMBH of the same mass in the total gravitational potential dictated also by the stellar bulge and dark-matter halo. We have then let loose a second $10^8 M_\odot$ SMBH 80 pc above the galactic plane in a nearly circular polar orbit and follow the evolution of the disk. Given that early-type galaxies share the same black-hole mass content (Ferrarese and Merritt 2000; Gebhardt *et al.* 2000), the interaction with a second SMBH of the same mass serves to explore in conservative way (without even considering the interaction with the stars around the second SMBH) the impact on the disk of a merging event with second galaxy of similar mass. Fig. 1 shows how after just 2.5 Myr the interaction with the alien SMBH has considerably disrupted the structure of the disk, which by becoming more vertically

⋆ E-mail: h.ledo@herts.ac.uk

extended and radially concentrated would be very hard to detect.

A systematic study of the incidence of NSD in early-type galaxies could therefore help constraining their assembling history, which, contrary to their star-formation history (e.g. Thomas *et al.* 2005), is poorly understood. According to the standard hierarchical paradigm for galaxy formation, the most massive galaxies should have been the last to reach their final configuration as they follow the merging paths of their host dark-matter haloes. The galactic environment should also play a role since once galaxies enter very crowded environments such as galaxy clusters it is more difficult for them to merge due to the high relative velocities with which they cross each other. These dependencies are illustrated in Fig. 2, which shows the predictions of the semi-analytical models of Khochfar and Silk (2006a,b) for the epoch of the last major merger experienced by galaxies of different masses and living in cluster or field environments. Semi-analytical models can also track whether the last merging events involved considerable amount of gas as well as the probability that a small gas-rich companion was subsequently acquired, which will then determine whether a NSD is found today. Numerical simulations (e.g. Hopkins and Quataert, submitted; Mayer *et al.* 2007; Barnes and Hernquist 1996) have indeed shown that when gas is involved in a merger event, it is always driven towards the centre of the remnant where it could then form a disk, depending on its angular momentum. NSDs could also provide constraints on the assembling history of their host galaxies in a more direct way, by dating the disk stellar population. In general, we expect the age of the stellar disk to represent a lower limit to the look-back time since the epoch of the last major merger event experienced by their host galaxy, since the NSD could have formed also after such an event, unless the last major merger was a gas rich event that led also to the formation of nuclear disk itself.

As a first step to use NSDs as tools to constrain the assembling history of early-type galaxies, in this paper we will provide for the first time a complete census of the nearby NSD population, providing also estimates for basic physical properties such as their mass and extent. This work will provide the basis for further investigations which will assess the fragility of the NSD identified here using a more comprehensive set of numerical simulations. Such set of fragile disks will constitute a sample for spectroscopic follow-up aimed at deriving their stellar ages, while the incidence of such fragile disks could be compared with the prediction of semi-analytical models.

This publication is organised as follows. To compile such a census we had to define a sample and retrieve the images (§2), to look for disks in these galaxies and to separate the disks from the bulges in order to find their properties (§3). The results will be presented in §4 and the conclusions in §5.

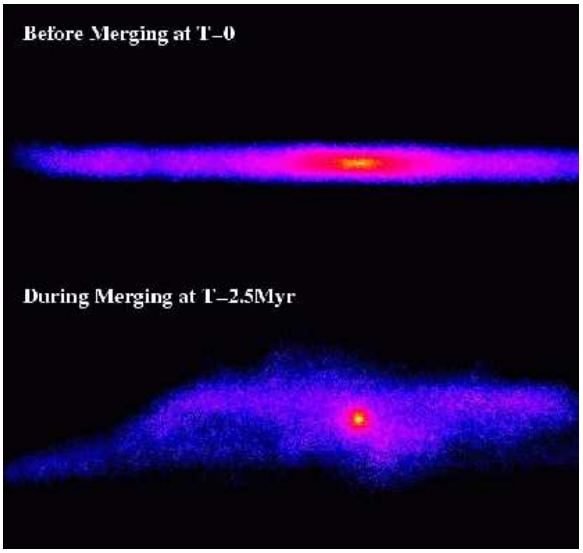

Figure 1. N-body simulation illustrating the fragility of nuclear stellar disks during major merger events. The top panel shows a stable nuclear disk 200 pc in diameter and 10^8 $M_\odot$ in mass that is orbiting a SMBH of the same mass in the total gravitational potential dictated also by the bulge and the dark matter particles, which are not shown for the sake of clarity. A second 10^8 $M_\odot$ SMBH is let loose in a nearly circular polar orbit 80 pc above the galactic plane, to simulate the impact with a second galaxy of similar mass. The lower panel illustrate the disruption suffered by the disk after just 2.5 Myr, which would be even greater if the bulge and dark matter particle from the incoming galaxy would have been included in the simulation.

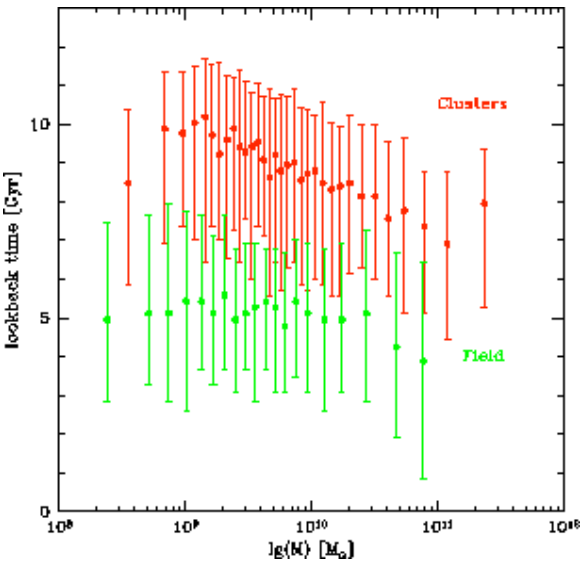

Figure 2. Prediction of semi-analytical models from Khochfar and Silk (2006a,b) for the age of the last major merger event experienced by galaxies of different masses and in different environments. Field early-type galaxies appear to have assembled later than those in clusters. In clusters, the models also predict a clear dependence on mass, with larger galaxies assembling later.

2 SAMPLE SELECTION AND DATA MINING

2.1 Selection and Acquisition

For this study we have selected, using the LEDA database (Paturel *et al.* 2003), all early-type galaxies (*E*, *E*-*S*0, *S*0

and *S0a*) within 100 Mpc so as to produce a volume-limited sample. This list was then cross-correlated with the HST archive and all the galaxies with images from the WFPC2 and ACS cameras were requested, preferably the filters F555W and F606W. In some cases these filters were not available and others had to be chosen. The use of different passbands should not bias our estimates of the disk inclination and extent, however, as shown by Morelli *et al.* (2010) nuclear disks do not present strong radial colour gradients. After downloading the available images they were checked for their quality and those saturated, too dusty or in which the galaxy was lying at the edge of the detector were discarded since in these cases it would have been impossible to find NSDs even if they were present. In the end we collected a sample of 466 early-type galaxies with HST images, out of a parent LEDA sample of 6801 galaxies.

2.2 Sample Properties

Having a sample, we retrieved the global parameters of our galaxies. Of particular interest are M_B and an estimate of the galactic environment, because they directly relate to the general questions we are trying to answer, and the galaxy inclination because it influences our ability to find the disks.The magnitude of our galaxies and an estimate for their inclination values are available from the LEDA database whereas to obtain a value for the galactic density we used the Nearby Galaxies Catalogue of Tully (1988).

Although the distribution of M_B and environment values for our HST sample and its parent LEDA sample are somewhat different this does not pose as a problem when we are dealing with the incidence of NSD. Indeed in this case it only matters that in each magnitude bin we have enough objects to obtain secure estimates for the NSD fraction. Also inclination differences do not matter for constraining the incidence of NSDs, as long as the distribution of inclination in each HST subsample allows a reliable correction of the fraction of NSD (that is if there are enough galaxies where the disk could have been detected, see §4.1.1). On the other hand we need to keep in mind that any conclusion on the structural properties of the NSDs, such as their typical size or mass, will be specific to our HST sample.

2.3 Inclination

The more face-on a disk is, the harder it is to identify it. Rix and White (1990) have studied this problem and concluded that for inclinations with $cos(i) > 0.6$ it is impossible to detect disky signatures in the galaxy isophotes. The inclination, i, is defined as being 0° for face-on disks and 90° if they are edge-on.

Although we do not know for sure the inclination of the nuclear disks, we will assume that the vast majority of them will have the same inclinations of their host galaxies, which is justified if we consider our sample galaxies as oblate axisymmetric spheroids. The LEDA database provides inclination estimates for the host galaxies based on the method applied by Heidmann *et al.* (1972) and Bottinelli *et al.* (1983). The inclination was calculated assuming all galaxies of a given Hubble type had an axis ratio equal to that observed in the flattest galaxy of that type. By construction, this method provides a conservative lower estimate for our galaxies' inclination, since intrinsically rounder galaxies in a given Hubble type would in reality have a higher inclination. Using such lower estimates to correct the fraction of NSD will lead to an upper limit on their incidence, whereas the uncorrected fraction provides a lower limit as if we were assuming that all galaxies where edge-on.

3 ANALYSIS

3.1 Disk Identification Process

Having collected the HST images of 466 early-type galaxies, we systematically searched for the signature of the presence of a NSD, both in maps for the fine structure of the galaxy and in the shape of the galaxy isophotes.
We have used the code of Pogge and Martini (2002) to generate structure maps for each of our sample galaxies, taking care to use in each case the appropriate WFPC2 or ACS point-spread function from the Tiny Tim code (Krist and Hook 2004).

We then fitted ellipses to the galaxy isophotes using the IRAF task *ellipse* and, in particular, extracted profiles for the galaxy ellipticity, ϵ, and the A_4 parameter which is the 4^{th} coefficient of the cosine term of the Fourier expansion of the considered isophotes (Carter 1977; Jedrzejewski 1987). In practice, the A_4 parameter measures the deviation of the isophote's shape from a perfect ellipse, and is positive in the case of disky deviations.

The existence of a disk in our galaxies is often revealed by the structure maps, but to separate disks from otherwise simply highly flattened central regions (e.g. a flattened bulge or a larger galactic-scale disk) we seek for a distinct peak in both the ϵ and A_4 profiles.

Figure 3 illustrates our disk-identification procedure for two sample galaxies, one with and one without a NSD. Similar figures for all the galaxies where we identified the presence of a nuclear disk are presented in Appendix A.

3.2 Disk-Bulge Decomposition

Having identified which galaxies in our sample host a NSD, we now wish to investigate the basic properties of such disks by disentangling their contribution to the observed surface brightness distribution of the host galaxy. For early-type galaxies where the main bulge component displays simple elliptical isophotes we can adopt the algorithm devised by Scorza and Bender (1995a), whereby the best disk parameters are sought by iteratively subtracting from the galaxy image an exponential disk model until the original signature of the disk is completely erased in the ϵ and A_4 profiles that are measured in the residual image. To perform the the Scorza & Bender decomposition on our sample nuclear disks we use the IDL implementation of this method of Morelli *et al.* (2004), where more details about the algorithm can be found.

Fig. 4 illustrates for the ESO507-027 how the disky deviations in the A_4 profile are minimised after the subtraction of the best exponential disk model. Appendix B shows similar figures for all NSD that were found embedded in an elliptical bulge, whereas Table A1 lists their basic parameters.

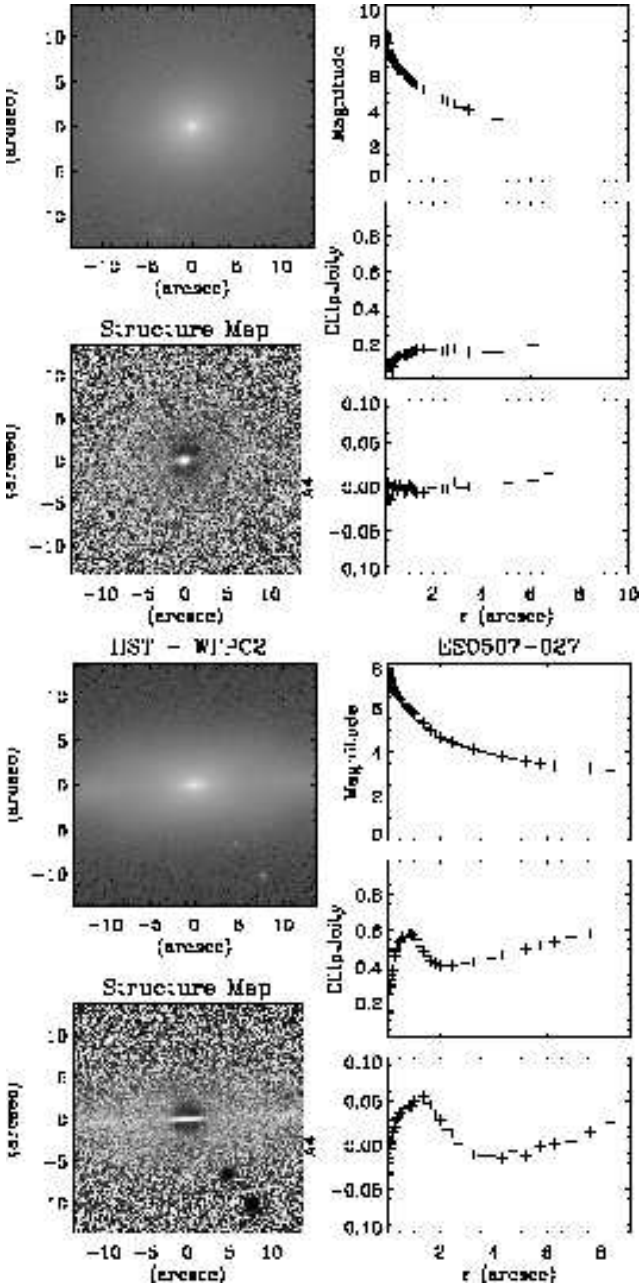

Figure 3. On the top panel we have the original image of NGC2592, its structure map and magnitude, ellipticity and A_4 profiles where no Nuclear Stellar Disk is visible and, on the bottom we have the same information for ESO507-027 where its presence is detected.

In a few cases we report the values for the disk parameters from previous studies.

3.3 Disk Size Estimates

For a large fraction of the NSD that we identified we could not apply the previously described technique efficiently, mostly owing to the presence of an intrinsically boxy bulge, in particular if the boxiness changes with radius, or dust. Under these circumstances we can at least estimate the extent of the NSD by exploiting the fact that the position of

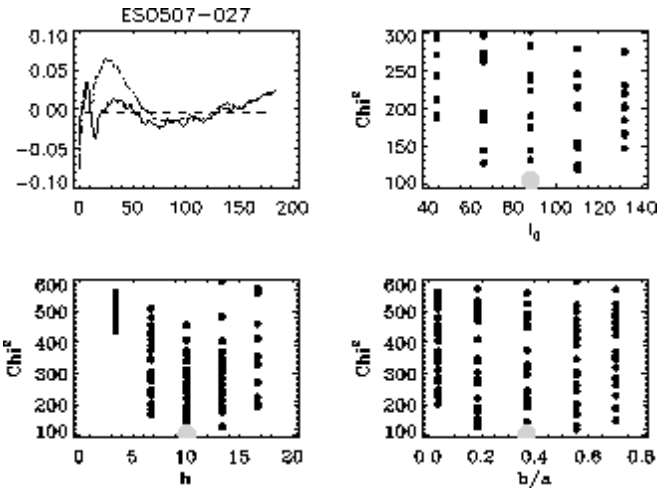

Figure 4. On the top left panel we can see A_4 profiles before (dot-dashed line) and after (solid line) Scorza and Bender decomposition for ESO507-027. The other three panels show the chosen parameters with their corresponding lower χ^2.

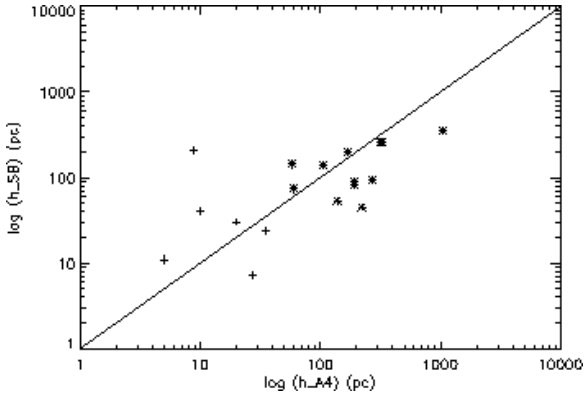

Figure 5. Relation between the sizes derived from the peak in the A_4 profile and those obtained from the Scorza and Bender decomposition. Asterisks represent the disks decomposed in this work and crosses show disks decomposed in previous works (Scorza and Bender 1995b; Scorza and van den Bosch 1998a; Morelli *et al.* 2004; van den Bosch *et al.* 1994b).

the peak of the A_4 deviation introduced by the disk correlates loosely with the actual extent of the disk, as found in the objects for which a disk-bulge decomposition has been performed (Fig. 5). This allowed us to estimate the sizes of the disks which could not be decomposed with the Scorza and Bender method. They are listed in Table A2.

4 RESULTS

4.1 The Census

By inspecting the structure maps and the isophotal shape of the central regions of 466 early-type galaxies we have found evidence for a distinct disk component in 63 objects, corresponding to 13.52% of our sample. Table 1 breaks down the observed fraction of NSDs as a function of galaxy type, whereas Tab. 2 and Tab. 3 show the incidence of NSDs as

function of the B-band absolute magnitude and galactic environment, when such quantities could be measured.

4.1.1 Inclination correction and Final Values

As mentioned in Sec 2.3, the inclination of the nuclear disks greatly affects our ability to detect them. It is indeed very likely that a considerable number of NSDs have escaped our detection because they lie in the equatorial plane of galaxies that are only slightly inclined from the plane of the sky, so that the NSDs appear close to face-on to us. The fraction of NSDs deduced directly from number of observed NSDs therefore represents only a lower limit for the true incidence of NSDs. We can estimate such true fraction considering that the number of NSDs that we have found should reflect the true fraction of NSD when considering only the systems where a NSDs could have in fact been detected, so that

$$f_{NSD} = \frac{f_{NSD,observed}}{f_{detectable,NSD}} \quad (1)$$

where $f_{NSD,observed}$ is the observed fraction of NSDs in the entire sample and $f_{detectable,NSD}$ is the fraction of galaxies where NSDs can be found. Using the estimates for the inclination of our sample galaxies that we retrieved in Sec 2.3, we can compute $f_{detectable,NSD}$ considering that according to Rix and White (1990) the ability to detect an embedded disk drops very quickly for $cos(i) > 0.6$, independent of the relative disk contribution to the total light distribution. Using the previous equation, the fraction of galaxies with $cos(i) < 0.6$ and considering that our inclination values are only lower estimates we can correct our face values for the incidence of NSDs and obtain upper limits for such fractions. These are also listed in Tabs. 1, 2 and 3.

Table 1 indicates that approximately between 13 and 23% of nearby early-type galaxies host nuclear stellar disks, without significant differences depending on their Hubble type. As regards the fraction of nuclear stellar disk as a function of their host absolute magnitude (Tab. 2), it would appear that the incidence of the disks peaks in the magnitude range between $M_B = -20$ and -18, decreasing sharply in particular towards higher stellar luminosity where no NSD is found. In fact even accounting for the smaller number of surveyed systems in the -24 to -22 magnitude bin we should have found between 1 and 4 objects to be consistent with the fraction estimated in the -22 to -20 bin. Finally, there appears to be no significant trend with environment, at least as defined in Tully (1988), although we need to keep in mind that unfortunately only less than half of our sample was found in this particular catalogue.

4.2 Properties of the Decomposed Disks

We have applied the Scorza & Bender disk-bulge decomposition to 12 disks, which doubles the number of NSD that were previously analysed in this way. Although a few more NSDs appeared embedded in well defined elliptical bulges, it was not possible to disentangle their light contribution. This is mainly because the observed A_4 profile does not appear to be well described by the simple model we used for the disks. Scorza and van den Bosch (1998b) compiled all previous measurements for the structural properties of NSDs and plotted them together with other kinds of galactic disks in a $\mu_c^0 - h$ plot which has later been updated by Morelli *et al.* (2004) and that we present in Figure 6, to which we now add our own 12 objects. Although our values fall within the range found in previous results, confirming that NSDs follow a similar $\mu_c^0 - h$ trend as embedded disks or main galactic disks, many of our decomposed NSDs appear to have a lower central surface brightness or smaller scale radius. In fact, the position of all NSDs in Fig . 6 suggests that these may follow a somewhat steeper and offset relation compared to bigger disks.

Type (1)	HST (2)	NSDs (3)	$f_{NSDs,obs}$ (4)	$f_{HST,detect}$ (5)	f_{NSDs} (6)
E	219	22	10.04±2.03	52.97	18.95±4
E-S0	68	9	13.24±4.11	63.24	20.9±6.2
S0	109	21	19.27±3.78	66.97	28.8±5.3
S0-a	70	11	15.71±4.35	64.29	24.44±6.8
Total	466	63	13.52±1.58	59.44	22.75±2.52

Table 1. As a function of galaxy Hubble type (1) the number of objects with HST images and of the NSDs found in them (2)-(3) yield a lower limit on the incidence of NSDs in early-type galaxies (4). Using the fraction of objects where disk detection is possible (5) we can correct for inclination biases and obtain an upper limit on the fraction of NSDs (6)

M_B (1)	HST (2)	NSDs (3)	$f_{NSDs,obs}$ (4)	$f_{HST,detect}$ (5)	f_{NSDs} (6)
-24 to -22	16	0	0	81.3	0
-22 to -20	175	23	13.1±2.6	59.4	22.1±4.1
-20 to -18	174	34	19.5±3.0	62.6	31.2±4.4
-18 to -16	70	6	8.6±3.4	51.4	16.7±6.2
-16 to -15	17	0	0	53.0	0

Table 2. Same as Tab. 1 but as a function of the galaxy absolute B-band magnitude (1), which was not available for 14 objects.

5 CONCLUSIONS

Nuclear stellar disks have long been regarded as common features in early-type galaxies, but a quantitative assessment of such statements was still lacking prior to this work. By performing the most extensive volume-limited census of NSDs to date we have now shown that between 13 to 23% of nearby early-type galaxies host such systems. The incidence of nuclear stellar disks appears to decline in the most massive systems, consistent with the expectations that dry mergers dominated the most recent history of such ob-

Density (1)	HST (2)	NSDs (3)	$f_{NSDs,obs}$ (4)	$f_{HST,detect}$ (5)	f_{NSDs} (6)
0-1	128	25	19.5±3.5	19.5	33.3±5.4
1-2	23	6	26.1±9.2	26.1	35.3±11.6
2-3	18	6	33.3±11.1	33.3	42.9±13.2
3-4	22	5	22.7±8.9	22.7	41.7±14.2

Table 3. Same as Tab. 1 but as a function of galactic environment (1), from Tully (1988). Only 191 objects were listed in this catalogue.

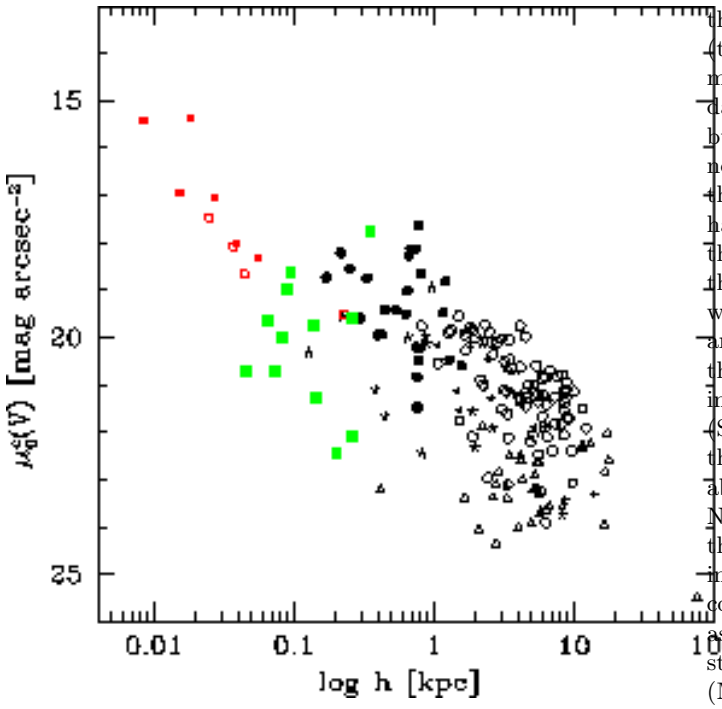

Figure 6. Disks $\mu_0^c - h$ diagram from Morelli *et al.* (2004). The open circles correspond to high surface-brightness spiral galaxies whereas low surface-brightness spirals are represented by triangles. Stars denote S0s and filled circles disky ellipticals. NSDs in elliptical and lenticular galaxies are indicated by filled squares and in spirals by open squares. The larger green squares are those added in this work and the smaller red ones are the pre-existing ones.

jects (Khochfar and Silk 2009; Khochfar and Burkert 2003) and also with the finding that NSDs are exceedingly rare in brightest cluster galaxies (2%, Laine *et al.* 2003). On the other hand, it is less clear what may cause the decrease in the fraction of NSDs that is found also at the faint end of our sample. Similarly, the lack of a dependence on galactic environment seems to contrast the first-order predictions of semi-analytical models (Fig. 2). In fact, according to these galaxies in clusters should have assembled much earlier and thus there should have been more time to regrow a nuclear disk. On the other hand, galaxies in cluster may not have ample reservoirs of cold gas at their disposal, in particular if orbiting within the hot-gas halo of the cluster, so that the early assembly of clusters does not make the presence of nuclear disks in cluster galaxies much more likely than in their field counterparts.

Using the well established technique of Scorza and Bender (1995a) to disentangle the light contribution of embedded disks from that of their surrounding bulges, we have extracted the structural parameters of 12 out of the 63 NSDs that we have identified. By doubling the number of NSDs we have shown even more convincingly that NSDs, like other kinds of large galactic disks, follow a correlation between the central surface brightness μ_c^0 and scale length h, although it would appear that NSDs obey a somewhat different relation with smaller scale lengths or fainter central surface brightness values. Considering that disk galaxies obey a very precise relation between their total luminosity and their maximum rotation velocity (the Tully-Fisher relation, Tully and Fisher (1977)) that may ultimately derive from the fact that they form in the dark matter halos that surround and dominate the mass budget of galaxies (Steinmetz and Navarro 1999), it may not be completely unexpected that NSDs, by forming in the central and bulge-dominated regions of galaxies, may have different structural and dynamical properties than that of their larger relatives. In fact, it is also possible that the structural properties of NSDs vary when dealing with different kinds of early-type galaxies such as disky and boxy systems (Kormendy and Bender 1996). Although the main reason for failing to isolate the disk component in the presence of a bulge of varying boxiness with radius (Sec 3.3) has mostly to do with an unclear a priori for the intrinsic A_4 profile that the bulge should have in the absence of a disk, we cannot exclude that in boxy ellipticals NSDs may have a different profile than exponential. Along the lines first suggested by Bender and Saglia (1999), NSDs in boxy ellipticals could be akin to the rapidly rotating components that in these objects are generally identified as kinematically decoupled cores, although in general such structure tend to extend over much larger scales than NSDs (McDermid *et al.* 2006), in particular for massive ellipticals with the oldest stellar populations.

Finally, although for the majority of the NSDs we could not clearly separate the disk and bulge contributions to the central light of their host galaxies, we have nonetheless estimated their sizes using as a reference radius the distance from the centre where the diskyness of the central isophotes appears to peak. Such scale length estimate, coupled with the $\mu_c^0 - h$ relation that NSDs appear also to obey and the N-body simulations, will be used in future investigations to assess which of our sample NSDs are indeed fragile against major merging events, thus providing good targets for a spectroscopic follow up aimed at constraining their stellar ages and thus, the time of their last major merger.

REFERENCES

Barnes, J. E. and Hernquist, L. (1996). Transformations of Galaxies. II. Gasdynamics in Merging Disk Galaxies. *ApJ*, **471**, 115–+.

Bender, R. and Saglia, R. P. (1999). Elliptical Galaxies: Detailed Structure, Scaling Relations and Formation. In D. R. Merritt, M. Valluri, & J. A. Sellwood, editor, *Galaxy Dynamics - A Rutgers Symposium*, volume 182 of *Astronomical Society of the Pacific Conference Series*, pages 113–+.

Bottinelli, L., Gouguenheim, L., Paturel, G., and de Vaucouleurs, G. (1983). H I line studies of galaxies. II - The 21-cm-width as an extragalactic distance indicator. *A&A*, **118**, 4–20.

Carter, D. (1977). Ph.D. thesis, , University of Cambridge, (1977).

Dotti, M., Colpi, M., Haardt, F., and Mayer, L. (2007). Supermassive black hole binaries in gaseous and stellar circumnuclear discs: orbital dynamics and gas accretion. *MNRAS*, **379**, 956–962.

Ferrarese, L. and Merritt, D. (2000). A Fundamental Relation between Supermassive Black Holes and Their Host Galaxies. *ApJ*, **539**, L9–L12.

Fouqué, P., Solanes, J. M., Sanchis, T., and Balkowski, C. (2001). Structure, mass and distance of the Virgo cluster from a Tolman-Bondi model. *A&A*, **375**, 770–780.

Gebhardt, K., Bender, R., Bower, G., Dressler, A., Faber, S. M., Filippenko, A. V., Green, R., Grillmair, C., Ho, L. C., Kormendy, J., Lauer, T. R., Magorrian, J., Pinkney, J., Richstone, D., and Tremaine, S. (2000). A Relationship between Nuclear Black Hole Mass and Galaxy Velocity Dispersion. *ApJ*, **539**, L13–L16.

Heidmann, J., Heidmann, N., and de Vaucouleurs, G. (1972). Inclination and absorption effects on the apparent diameters, optical luminosities and neutral hydrogen radiation of galaxies-I, Optical and 21-cm line data. *MmRAS*, **75**, 85–+.

Hopkins, P. F. and Quataert, E. (2010). How Do Massive Black Holes Get Their Mass. *MNRAS*.

Jedrzejewski, R. I. (1987). CCD surface photometry of elliptical galaxies. I - Observations, reduction and results. *MNRAS*, **226**, 747–768.

Khochfar, S. and Burkert, A. (2003). The Importance of Spheroidal and Mixed Mergers for Early-Type Galaxy Formation. *ApJ*, **597**, L117–L120.

Khochfar, S. and Silk, J. (2006a). A Simple Model for the Size Evolution of Elliptical Galaxies. *ApJ*, **648**, L21–L24.

Khochfar, S. and Silk, J. (2006b). On the origin of stars in bulges and elliptical galaxies. *MNRAS*, **370**, 902–910.

Khochfar, S. and Silk, J. (2009). Dry mergers: a crucial test for galaxy formation. *MNRAS*, **397**, 506–510.

Kormendy, J. and Bender, R. (1996). A Proposed Revision of the Hubble Sequence for Elliptical Galaxies. *ApJ*, **464**, L119+.

Krist, C. and Hook, R. (2004). *Tiny Tim User's Guide*.

Laine, S., van der Marel, R. P., Lauer, T. R., Postman, M., O'Dea, C. P., and Owen, F. N. (2003). Hubble Space Telescope Imaging of Brightest Cluster Galaxies. *AJ*, **125**, 478–505.

Mayer, L., Kazantzidis, S., Madau, P., Colpi, M., Quinn, T., and Wadsley, J. (2007). Rapid Formation of Supermassive Black Hole Binaries in Galaxy Mergers with Gas. *Science*, **316**, 1874–.

McDermid, R. M., Emsellem, E., Shapiro, K. L., Bacon, R., Bureau, M., Cappellari, M., Davies, R. L., de Zeeuw, T., Falcón-Barroso, J., Krajnović, D., Kuntschner, H., Peletier, R. F., and Sarzi, M. (2006). The SAURON project - VIII. OASIS/CFHT integral-field spectroscopy of elliptical and lenticular galaxy centres. *MNRAS*, **373**, 906–958.

Morelli, L., Halliday, C., Corsini, E. M., Pizzella, A., Thomas, D., Saglia, R. P., Davies, R. L., Bender, R., Birkinshaw, M., and Bertola, F. (2004). Nuclear stellar discs in low-luminosity elliptical galaxies: NGC 4458 and 4478. *MNRAS*, **354**, 753–762.

Morelli, L., Cesetti, M., Corsini, E. M., Pizzella, A., Dalla Bontà, E., Sarzi, M., and Bertola, F. (2010). Multiband photometric decomposition of nuclear stellar disks. *ArXiv e-prints*.

Paturel, G., Petit, C., Prugniel, P., Theureau, G., Rousseau, J., Brouty, M., Dubois, P., and Cambrésy, L. (2003). HYPERLEDA. I. Identification and designation of galaxies. *A&A*, **412**, 45–55.

Pizzella, A., Corsini, E. M., Morelli, L., Sarzi, M., Scarlata, C., Stiavelli, M., and Bertola, F. (2002). Nuclear Stellar Disks in Spiral Galaxies. *ApJ*, **573**, 131–137.

Pogge, R. W. and Martini, P. (2002). Hubble Space Telescope Imaging of the Circumnuclear Environments of the CfA Seyfert Galaxies: Nuclear Spirals and Fueling. *ApJ*, **569**, 624–640.

Rest, A., van den Bosch, F. C., Jaffe, W., Tran, H., Tsvetanov, Z., Ford, H. C., Davies, J., and Schafer, J. (2001). WFPC2 Images of the Central Regions of Early-Type Galaxies. I. The Data. *AJ*, **121**, 2431–2482.

Rix, H.-W. and White, S. D. M. (1990). Disks in elliptical galaxies. *ApJ*, **362**, 52–58.

Scorza, C. and Bender, R. (1995a). The internal structure of disky elliptical galaxies. *A&A*, **293**, 20–43.

Scorza, C. and Bender, R. (1995b). The internal structure of disky elliptical galaxies. *A&A*, **293**, 20–43.

Scorza, C. and van den Bosch, F. C. (1998a). Nuclear stellar discs in early-type galaxies - II. Photometric properties. *MNRAS*, **300**, 469–478.

Scorza, C. and van den Bosch, F. C. (1998b). Nuclear stellar discs in early-type galaxies - II. Photometric properties. *MNRAS*, **300**, 469–478.

Steinmetz, M. and Navarro, J. F. (1999). The Cosmological Origin of the Tully-Fisher Relation. *ApJ*, **513**, 555–560.

Thomas, D., Maraston, C., Bender, R., and Mendes de Oliveira, C. (2005). The Epochs of Early-Type Galaxy Formation as a Function of Environment. *ApJ*, **621**, 673–694.

Tully, R. B. (1988). *Nearby galaxies catalog*.

Tully, R. B. and Fisher, J. R. (1977). A new method of determining distances to galaxies. *A&A*, **54**, 661–673.

van den Bosch, F. C. and de Zeeuw, P. T. (1996). Self-Consistent, Axisymmetric Two-Integral Models of Elliptical Galaxies with Embedded Nuclear Discs. *MNRAS*, **283**, 381–399.

van den Bosch, F. C., Ferrarese, L., Jaffe, W., Ford, H. C., and O'Connell, R. W. (1994a). Hubble Space Telescope photometry of the central regions of Virgo cluster elliptical galaxies. II: Isophote shapes. *AJ*, **108**, 1579–1597.

van den Bosch, F. C., Ferrarese, L., Jaffe, W., Ford, H. C., and O'Connell, R. W. (1994b). Hubble Space Telescope photometry of the central regions of Virgo cluster elliptical galaxies. II: Isophote shapes. *AJ*, **108**, 1579–1597.

APPENDIX A: NUCLEAR STELLAR DISKS

A1 Properties of the Galaxies With Disks

Table A1. Properties of the decomposed disks where h is the scale-length, the inclination is as defined in §2.3 and $\mu^c_{0,V}$ is the central surface brightness.

Galaxy name	**h** (pc)	**inclination** (°)	$\boldsymbol{\mu^c_{0,V}}$ (mag arcsec^{-2})
ESO352-057	$44.74\pm^{23.16}_{16.05}$	$76.26\pm^{8.58}_{22.42}$	$20.74\pm^{1.05}_{1.04}$
ESO378-020	$53.39\pm^{33.51}_{18.54}$	$65.98\pm^{16.78}_{19.69}$	$19.1\pm^{1.27}_{0.58}$
ESO507-027	$94.87\pm^{23.22}_{16.8}$	$68.28\pm^{7.83}_{9.61}$	$18.61\pm^{0.47}_{0.37}$
IC0875	$259.67\pm^{59.41}_{77.71}$	$84.84\pm^{2.29}_{2.31}$	$22.08\pm^{0.63}_{0.4}$
NGC0584	$90.18\pm^{24.82}_{18.37}$	$73.86\pm^{6.93}_{4.96}$	$18.97\pm^{0.6}_{0.28}$
NGC3385	$351.19\pm^{52.33}_{55.07}$	$61.71\pm^{1.55}_{5.08}$	$17.78\pm^{0.06}_{0.16}$
NGC3610	$260.38\pm^{44.81}_{79.84}$	$81.81\pm^{4.19}_{1.6}$	$19.60\pm^{0.77}_{0.2}$
NGC4128	$138.01\pm^{43.84}_{38.68}$	$85.76\pm^{1.95}_{0.92}$	$19.77\pm^{0.67}_{0.21}$
NGC4474	$143.5\pm^{59.28}_{59.21}$	$86.49\pm^{2.36}_{2.23}$	$21.29\pm^{1.21}_{0.54}$
NGC4621	$73.87\pm^{13.71}_{24.26}$	$83.97\pm^{2.59}_{2.02}$	$20.72\pm^{0.6}_{0.32}$
NGC4660	$81.19\pm^{12.32}_{27.19}$	$78.92\pm^{4.19}_{3.99}$	$20.02\pm^{0.51}_{0.33}$
NGC5308[a]	$201.59\pm^{30.21}_{45.56}$	$89.89\pm^{-}_{-}$	$22.46\pm^{-}_{-}$

[a] We were unable to derive the errors for the inclination.

Table A2. Galaxies where disks were found and some of their properties. (1) Galaxy's name; (2) Hubble type; (3) $\log_{10}$ of the axis ratio; (4) $\log_{10}$ of the apparent major axis diameter d25 at 25 mag.arcsec^{-2}; (5) disk inclination; (6) absolute B-magnitude; (7) radial velocity corrected for Local Group infall towards Virgo (208 kms^{-1}); (8) Distance derived from (7) and assuming H_0=72 kms^{-1} Mpc^{-1}, except for Virgo cluster members for which we adopted a common distance of 18 Mpc (Fouqué *et al.* 2001); (9) Density from Tully (1988); (10) Disk size with the indication in (11) of the source of the values, where *M* are those measured with the decomposition procedure, *E* have been estimated using the peak of the A_4 and *L* come from the literature.

Name	**Type**	**logr$_{25}$**	**logd$_{25}$**	**inclination (^{o})**	**mabs**	**V_vir (kms^{-1})**	**distance (Mpc)**	**Density (Mpc^{-3})**	**Disk size (pc)**	**Source**
(1)	(2)	(3)	(4)	(5)	(6)	(7)	(8)	(9)	(10)	(11)
ESO352-057	S0	0.327	1.014	82.98	-19.842	5736.2	76.11	-	44.74	M
ESO378-020	S0	0.243	1.186	68.17	-19.899	5479.7	39.87	-	53.39	M
ESO507-027	S0	0.682	1.251	90.0	-20.079	2870.7	43.27	-	94.87	M
IC0875	S0	0.234	1.16	67.23	-19.442	3115.4	42.32	-	259.67	M
NGC0584	E	0.179	1.578	79.78	-20.891	3047.0	24.49	0.42	90.18	M
NGC1023	E-S0	0.377	1.868	76.7	-20.914	769.9	10.69	0.57	57	E
NGC1129	E	0.42	1.444	90.0	-21.604	5404.8	75.07	-	146	E
NGC1351	E-S0	0.189	1.532	65.35	-19.004	1301.0	18.07	1.57	131	E
NGC1381	S0	0.421	1.405	90.0	-19.338	1520.6	21.12	1.54	131	E
NGC1426	E	0.175	1.457	78.27	-19.092	1263.2	17.54	0.66	43	E
NGC1427	E	0.179	1.636	71.35	-19.399	1159.2	16.10	1.59	16	E
NGC1439	E	0.02	1.473	23.03	-19.507	1486.8	20.65	0.45	130	E
NGC2549	S0	0.594	1.563	90.0	-19.445	1248.6	17.34	0.13	42	E
NGC2685	S0-a	0.272	1.636	68.79	-19.092	1094.2	15.2	0.13	66	E
NGC2787	S0-a	0.249	1.510	65.86	-19.645	949.0	13.18	0.06	115	E
NGC2865	E	0.082	1.382	45.2	-20.792	2578.8	35.82	0.11	191	E
NGC3115	E-S0	0.383	1.916	81.6	-20.042	642.6	8.93	0.08	30.0	L[1]
NGC3156	S0	0.28	1.282	79.15	-18.512	1340.3	18.62	0.2	63	E
NGC3377	E	0.327	1.588	90.0	-19.163	744.5	10.34	0.49	35	E
NGC3384	E-S0	0.349	1.717	90.0	-19.826	917.1	12.74	0.54	49	E
NGC3385	S0	0.267	1.182	72.56	-21.927	7824.4	108.67	-	351.19	M
NGC3610	E	0.027	1.375	25.95	-20.664	1943.4	26.99	0.3	260.38	M
NGC3613	E	0.315	1.544	90.0	-20.864	2232.9	31.01	-	15	E
NGC3706	E-S0	0.167	1.477	61.64	-21.117	2817.9	39.14	0.27	114	E
NGC3818	E	0.199	1.387	90.0	-19.389	1678.7	23.32	0.2	23	E
NGC3900	S0-a	0.311	1.413	70.82	-20.168	1942.8	26.98	0.13	-	E
NGC3945	S0-a	0.227	1.744	63.17	-20.085	1496.5	20.78	0.5	50	E
NGC4026	S0	0.702	1.644	90.0	-19.592	1206.5	16.76	1.71	41	E
NGC4128	S0	0.519	1.344	90.0	-20.041	2591.1	36.0	0.27	138.01	M
NGC4270	S0	0.392	1.269	72.8	-19.702	2414.3	18.0	0.83	43.63	E
NGC4318	E	0.167	0.869	79.12	-17.285	1297.6	18.02	1.47	70	E
NGC4342	E-S0	0.297	1.101	90.0	-16.954	810.7	11.26	2.64	7.3	L[2]
NGC4352	S0	0.331	1.231	90.0	-19.056	2164.4	18.0	-	17.45	E
NGC4458	E	0.03	1.204	28.77	-17.437	770.0	10.69	3.21	11.0	L[3]
NGC4473	E	0.235	1.630	90.0	-21.707	2338.1	18.0	2.17	183.26	E
NGC4474	S0	0.174	1.368	57.3	-19.652	1707.6	18.0	3.8	143.5	M
NGC4478	E	0.089	1.243	50.85	-19.602	1479.7	20.55	3.92	40.5	L[3]
NGC4483	S0-a	0.282	1.265	71.34	-17.632	958.3	13.31	3.83	13	E
NGC4515	E-S0	0.099	1.123	45.77	-17.775	1059.8	14.72	-	36	E
NGC4528	S0	0.271	1.208	73.43	-18.874	1453.4	20.19	-	10	E
NGC4546	E-S0	0.254	1.510	75.96	-19.726	1064.1	14.78	0.27	43	E
NGC4570	S0	0.618	1.597	90.0	-20.444	1813.0	18.0	2.66	23.5	L[2]
NGC4621	E	0.152	1.658	71.93	-20.789	527.1	18.0	2.6	73.87	M
NGC4623	S0-a	0.477	1.352	90.0	-19.005	1863.7	18.0	2.36	210	L[4]
NGC4660	E	0.124	1.323	61.24	-19.241	1185.1	18.0	3.37	81.19	M
NGC4742	E	0.191	1.358	90.0	-19.376	1257.0	17.46	0.73	51	E
NGC4762	S0	0.37	1.917	90.0	-19.921	1065.4	18.0	2.65	226.89	E
NGC4866	S0-a	0.768	1.761	90.0	-20.727	2095.8	18.0	1.08	26.18	E
NGC5076	S0-a	0.138	1.126	48.83	-19.491	2975.3	41.32	-	621	E
NGC5252	S0	0.233	1.111	67.18	-21.039	6967.0	96.76	-	-	E
NGC5308	S0	0.877	1.642	90.0	-20.439	2279.5	31.66	0.45	201.59	M

[1] Scorza and Bender (1995b)
[2] Scorza and van den Bosch (1998a)
[3] Morelli *et al.* (2004)
[4] van den Bosch *et al.* (1994b)

Table A3. Continuation of properties table.

Name	**Type**	**logr$_{25}$**	**logd$_{25}$**	**inclination (^{o})**	**mabs**	**V_vir (kms^{-1})**	**distance (Mpc)**	**Density (Mpc^{-3})**	**Disk size (pc)**	**Source**
(1)	(2)	(3)	(4)	(5)	(6)	(7)	(8)	(9)	(10)	(11)
NGC5854	S0-a	0.58	1.483	90.0	-19.698	1833.0	25.46	0.74	148	E
NGC7173	E	0.088	1.275	47.16	-19.897	2368.8	32.90	0.35	48	E
NGC7176	E	0.024	1.569	25.29	-20.423	2387.5	33.16	0.39	64	E
NGC7562	E	0.137	1.338	67.29	-21.427	3571.8	49.61	-	-	E
NGC7585	S0-a	0.123	1.406	46.52	-21.291	3432.0	47.67	-	69	E
NGC7619	E	0.106	1.407	56.04	-21.987	3798.5	52.76	-	256	E
NGC7785	E	0.283	1.447	90.0	-21.411	3875.7	53.83	-	497	E
PGC013343	E-S0	0.039	1.030	28.55	-16.909	1486.7	20.65	-	100	E
PGC036465	S0-a	0.307	0.825	67.59	-19.656	5736.2	79.67	-	232	E
PGC044815	S0	0.35	0.7	90.0	-18.58	6784	94.22	-	1005	E
UGC01003	S0	0.346	0.922	90.0	-19.488	5192.1	72.11	-	105	E
UGC03426	S0	0.096	1.224	42.78	-20.869	4292.5	59.62	-	58	E

A2 NSD Structure Maps, Ellipticity and A_4 profiles

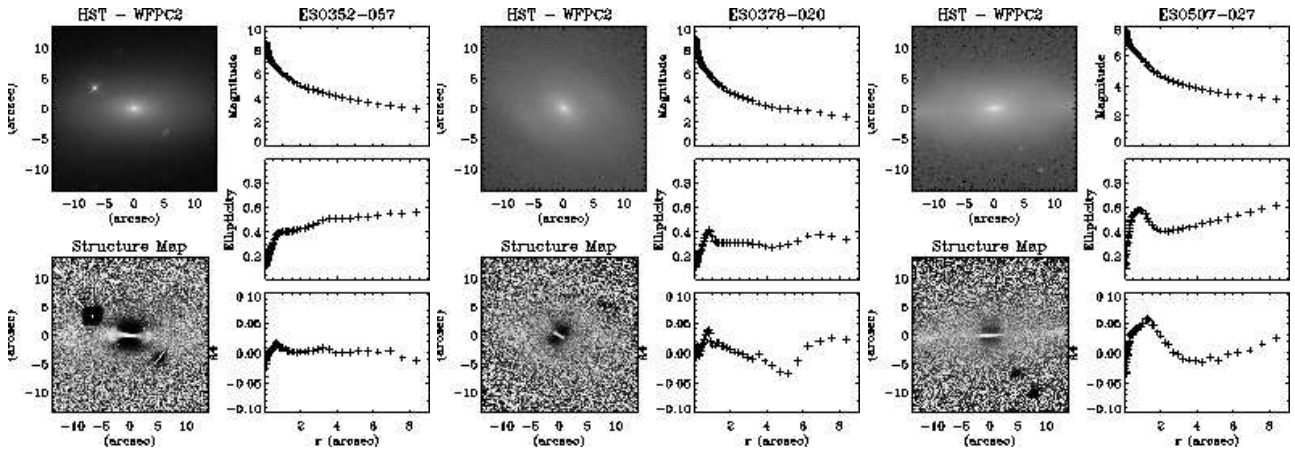

Figure A1. ESO352-057 on the left panel, in the middle ESO378-020 and ESO507-027 at the right. The original images and the structure maps are shown on the left of each panel and on the right we can see the surface brightness, ellipticity and A_4 profiles.

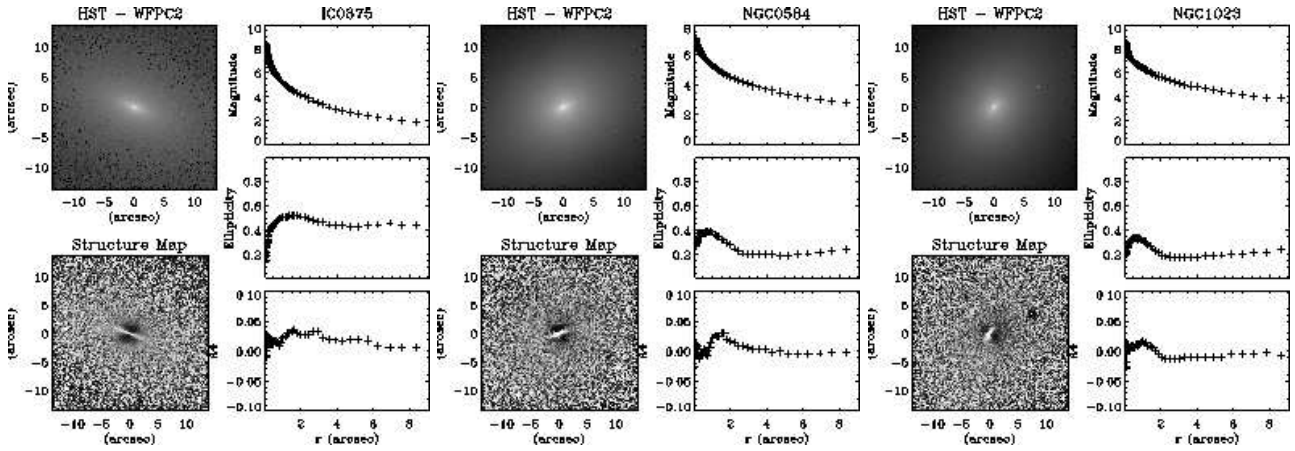

Figure A2. IC0875 on the left, NGC0584 in the middle and NGC1023 on the right.

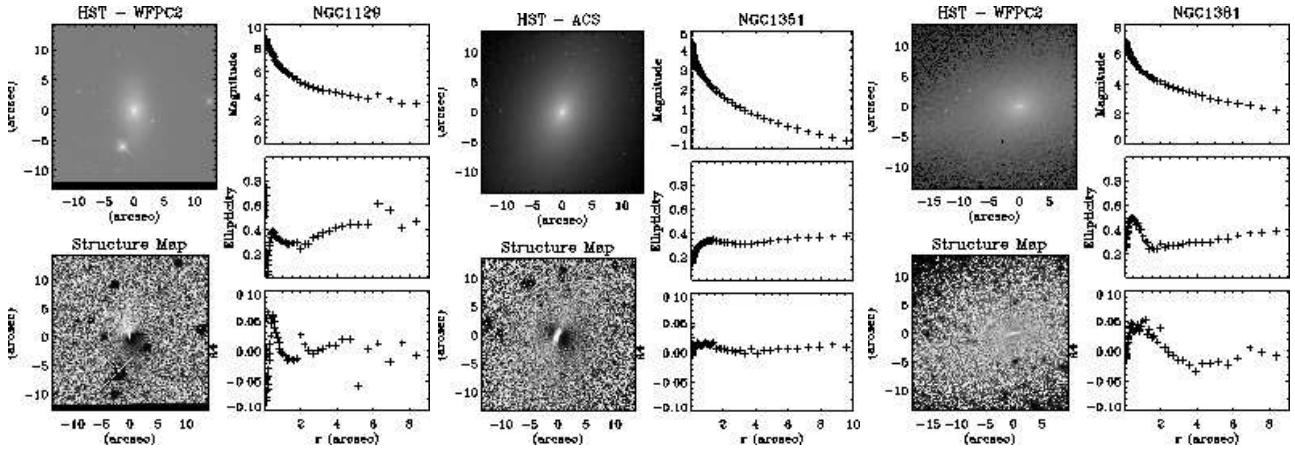

Figure A3. NGC1129 on the left, NGC1351 in the middle and NGC1381 on the right.

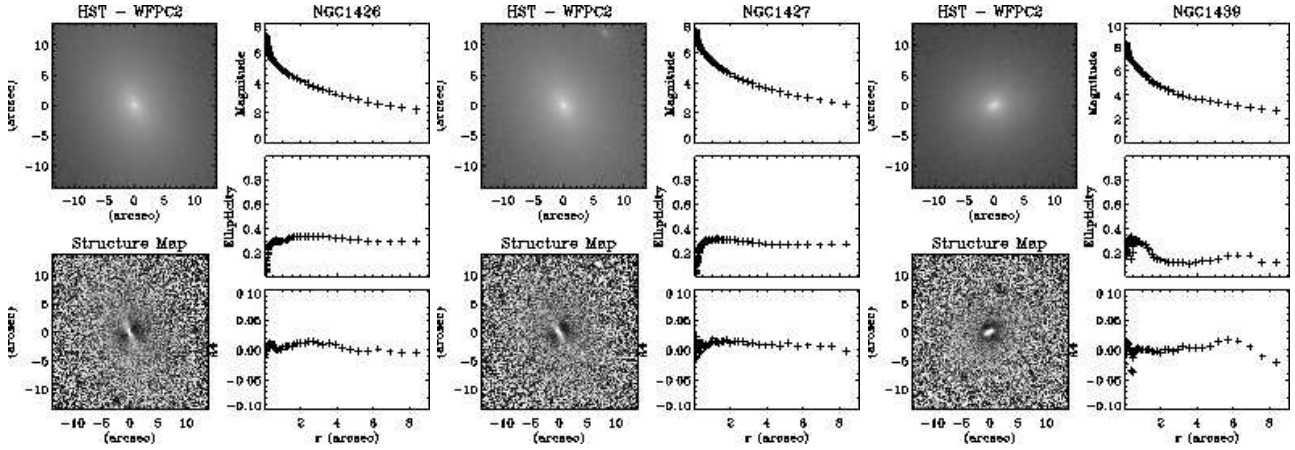

Figure A4. NGC1426 on the left, NGC1427 in the middle and NGC1439 on the right.

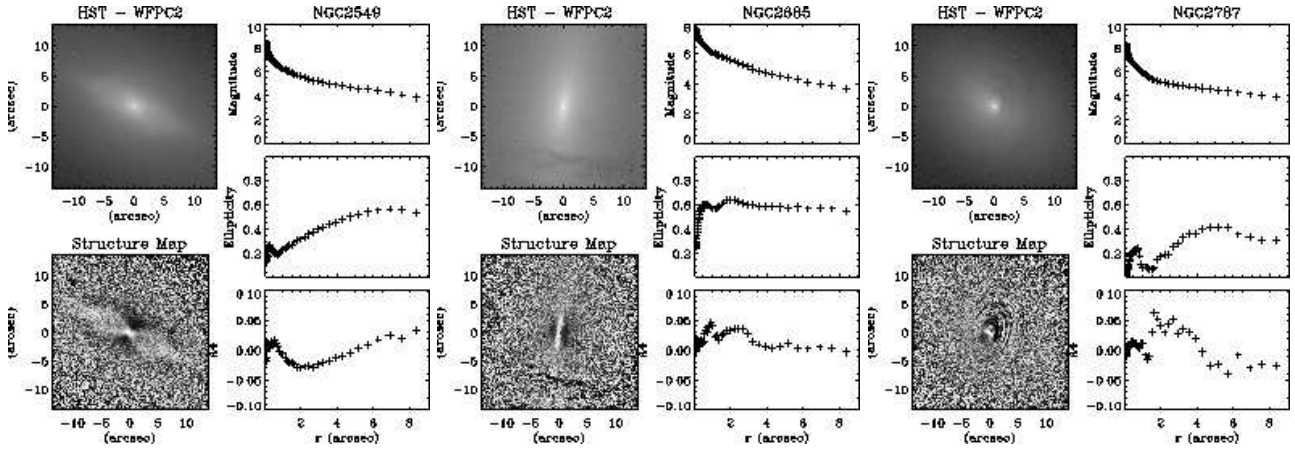

Figure A5. NGC2549 on the left, NGC2685 in the middle and NGC2787 on the right.

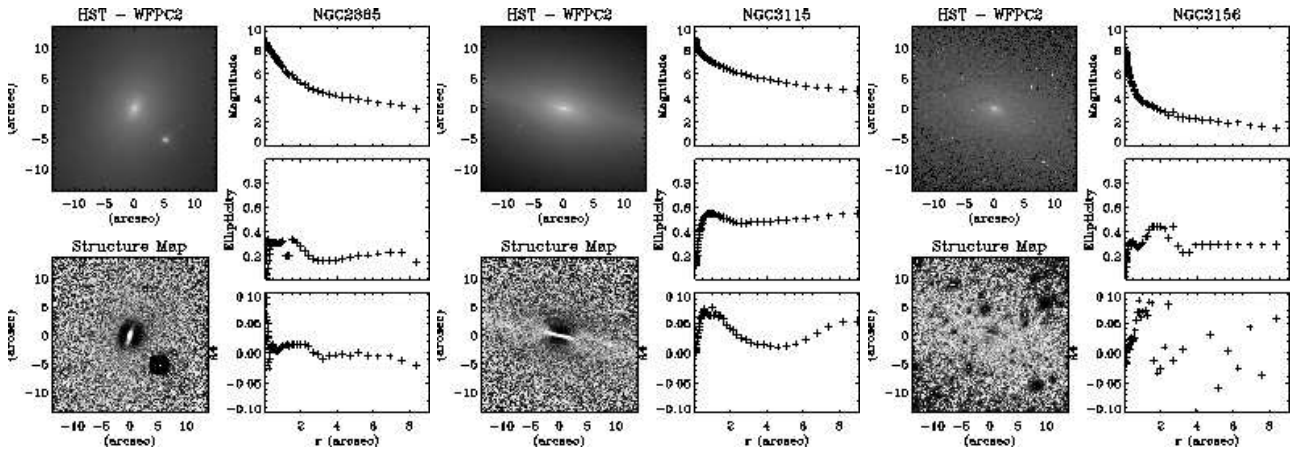

Figure A6. NGC2865 on the left, NGC3115 in the middle and NGC3156 on the right.

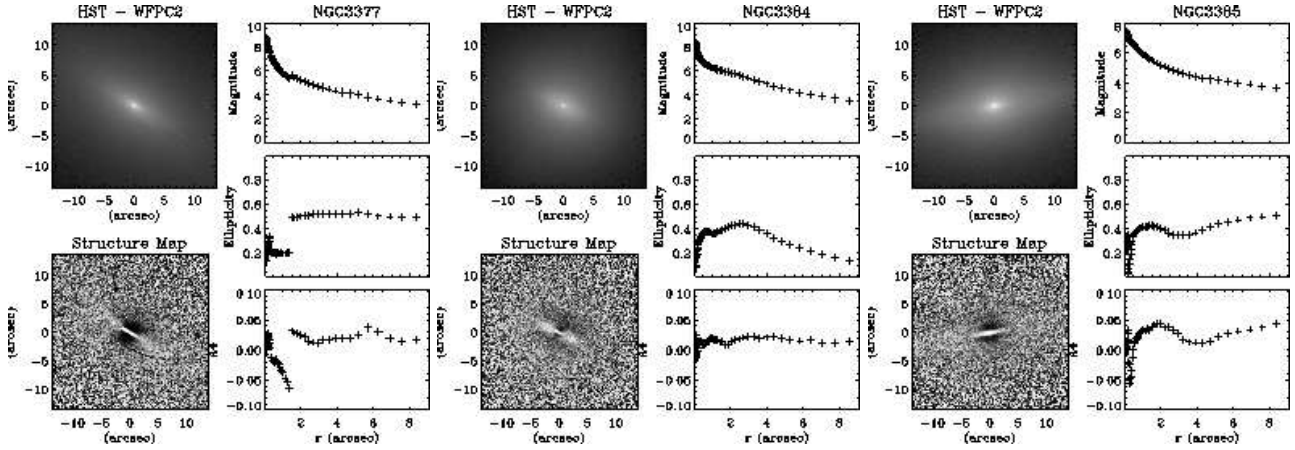

Figure A7. NGC3377 on the left, NGC3384 in the middle and NGC3385 on the right.

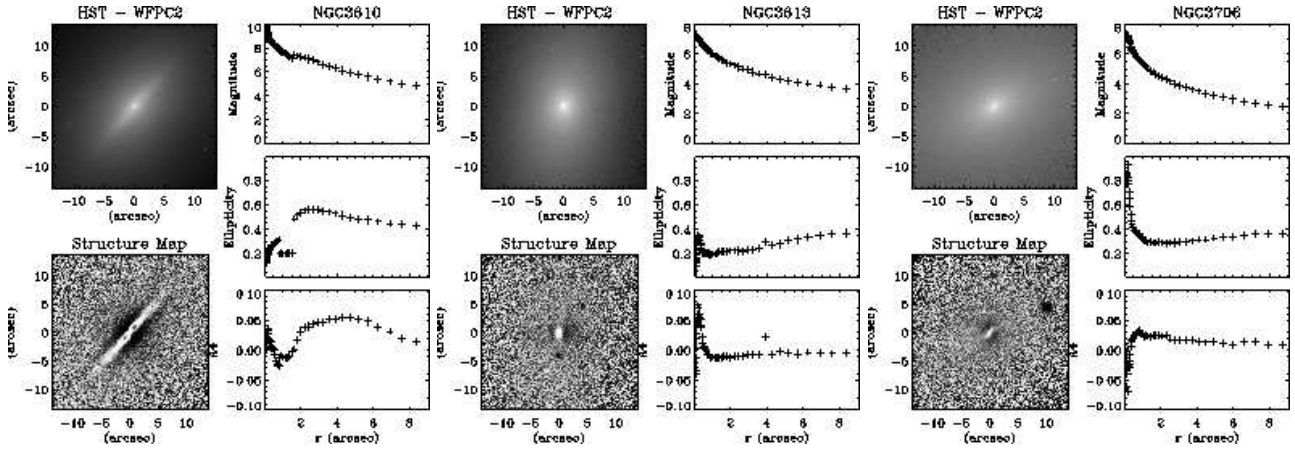

Figure A8. NGC3610 on the left, NGC3613 in the middle and NGC3706 on the right.

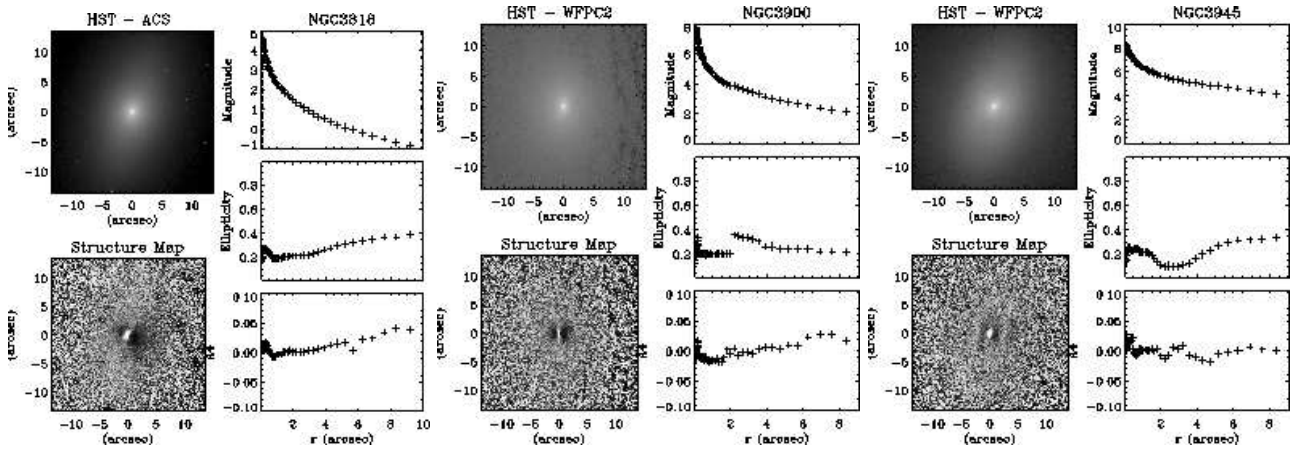

Figure A9. NGC3818 on the left, NGC3900 in the middle and NGC3945 on the right.

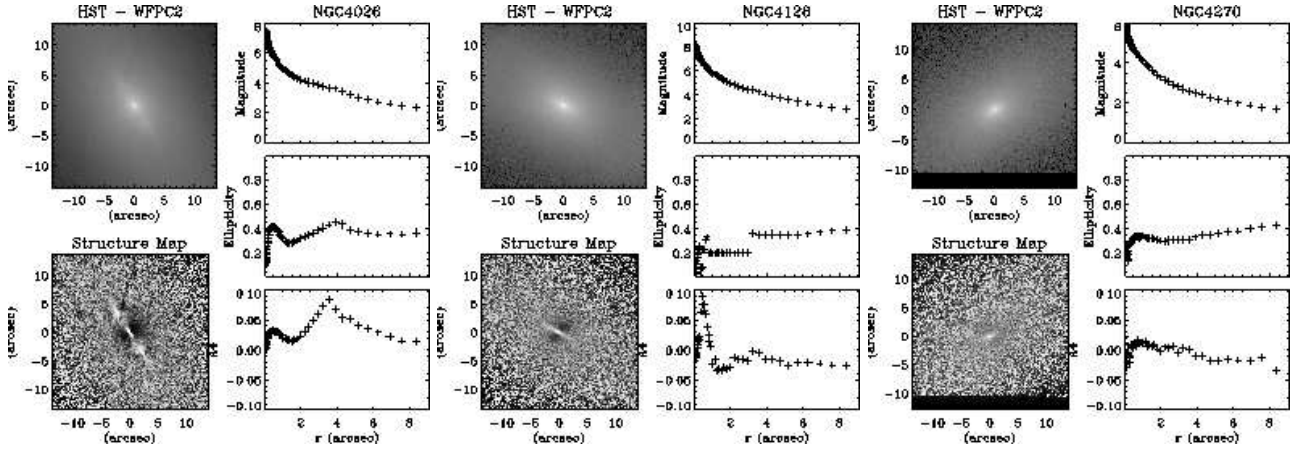

Figure A10. NGC4026 on the left, NGC4128 in the middle and NGC4270 on the right.

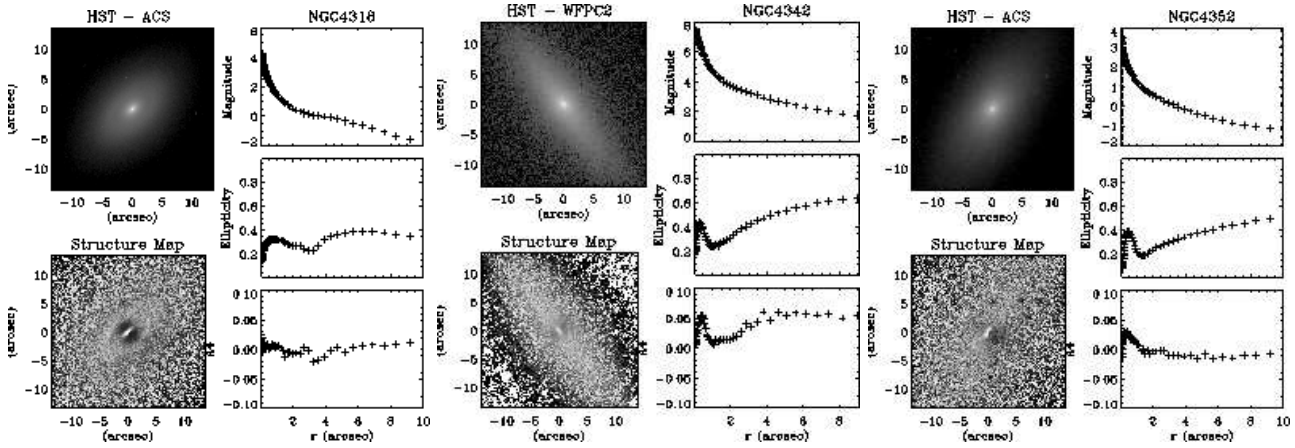

Figure A11. NGC4318 on the left, NGC4342 in the middle and NGC4352 on the right.

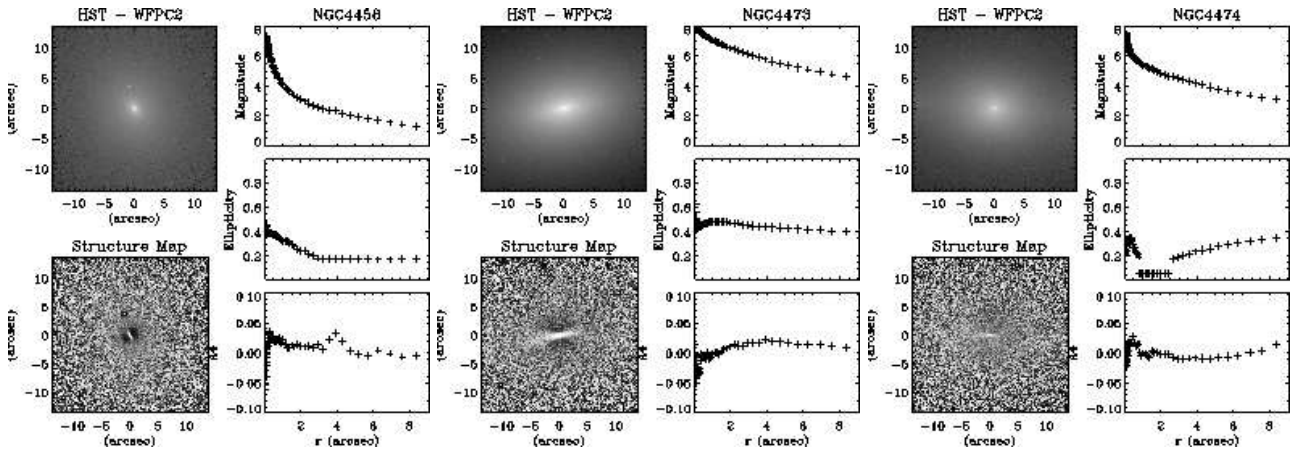

Figure A12. NGC4458 on the left, NGC4473 in the middle and NGC4474 on the right.

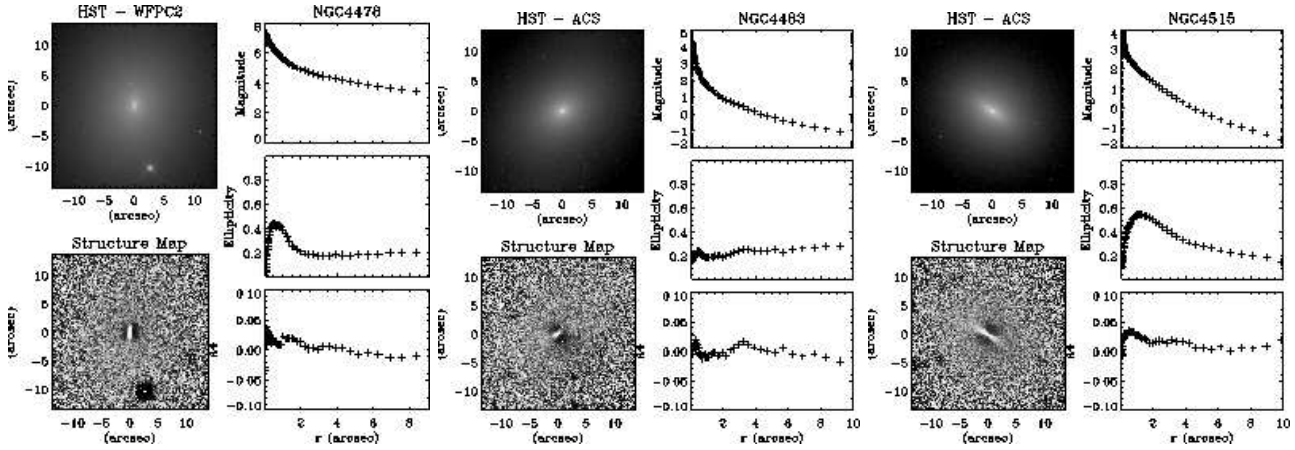

Figure A13. NGC4478 on the left, NGC4483 in the middle and NGC4515 on the right.

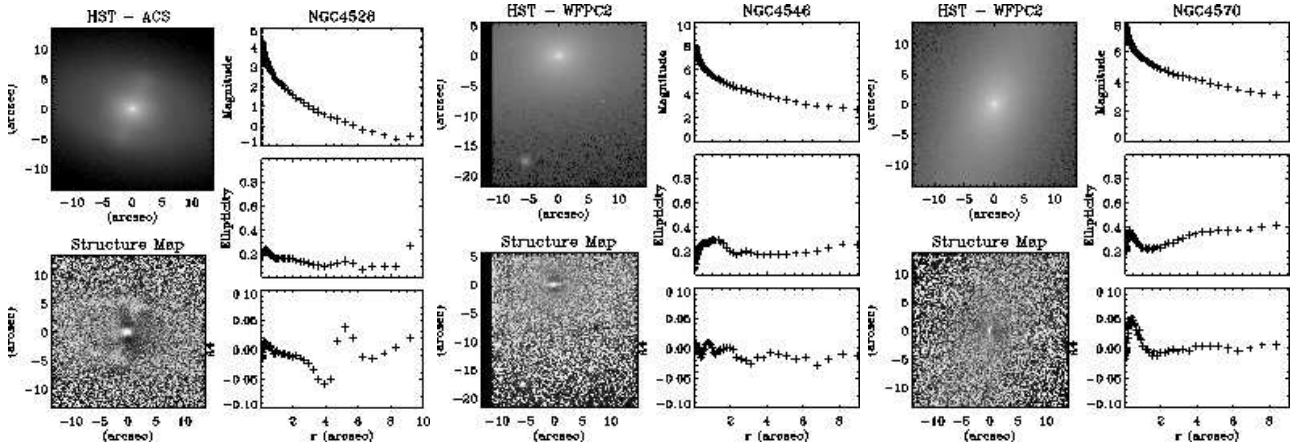

Figure A14. NGC4528 on the left, NGC4546 in the middle and NGC4570 on the right.

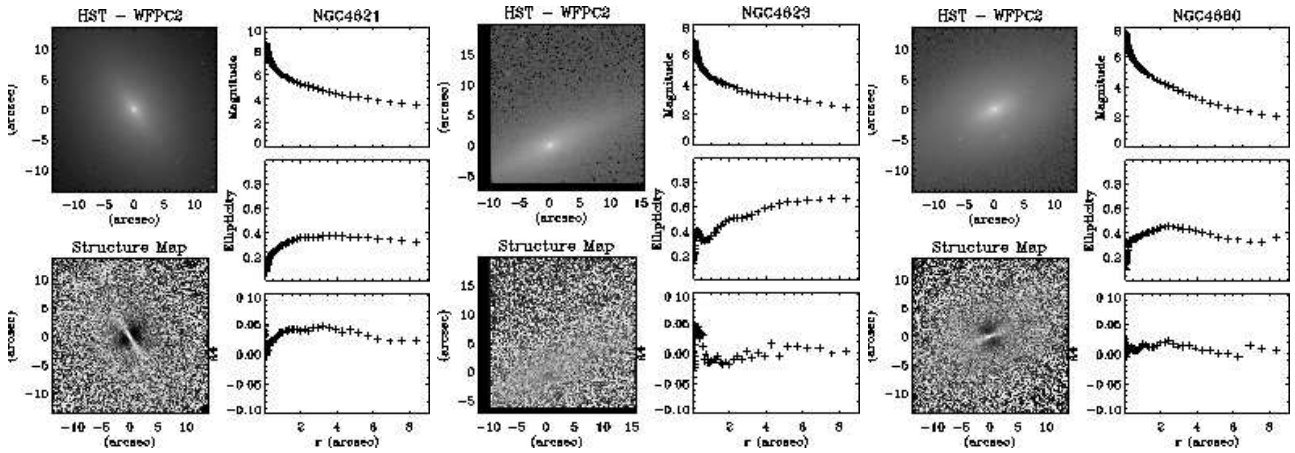

Figure A15. NGC4621 on the left, NGC4623 in the middle and NGC4660 on the right.

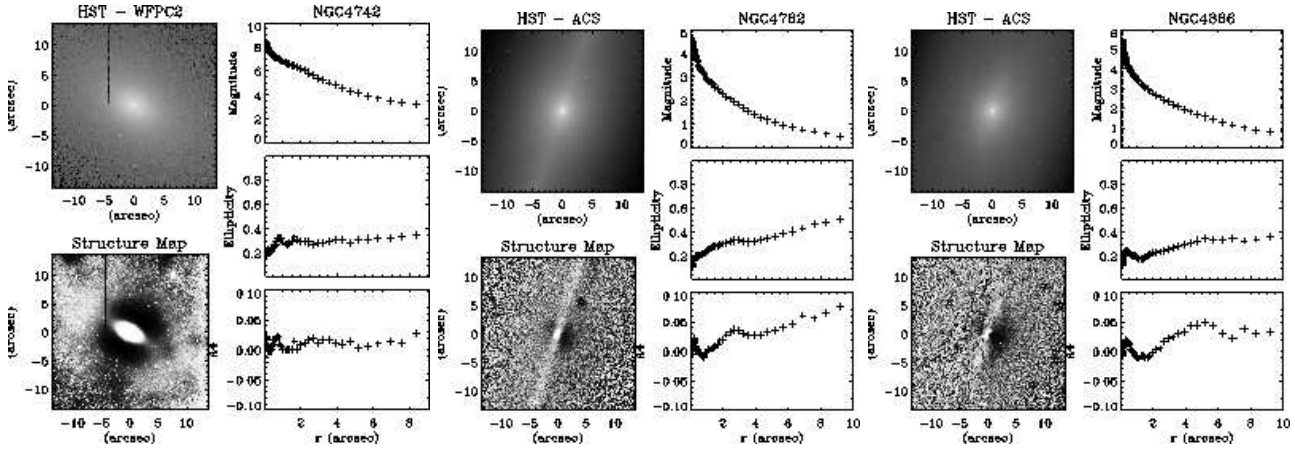

Figure A16. NGC4742 on the left, NGC4762 in the middle and NGC4866 on the right.

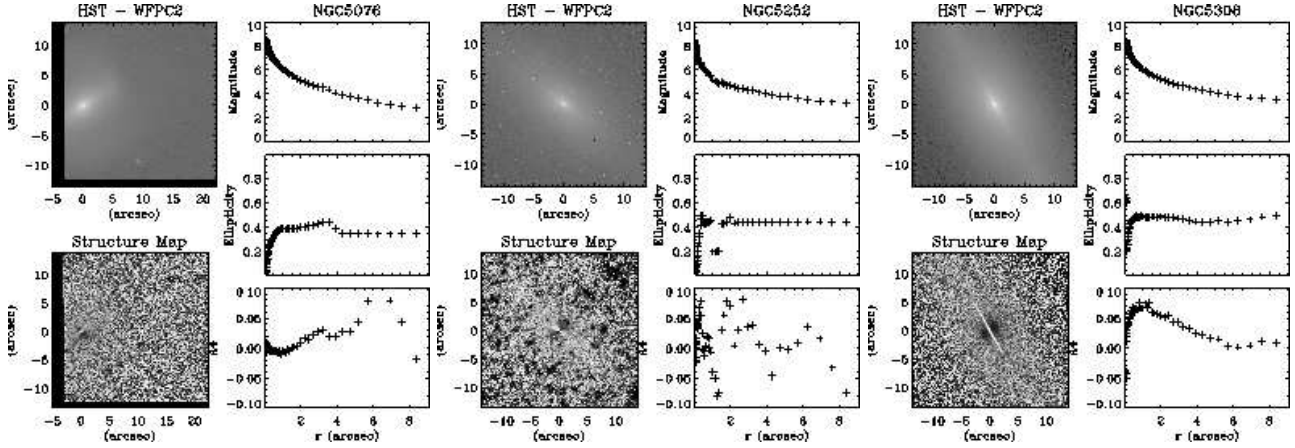

Figure A17. NGC5076 on the left, NGC5252 in the middle and NGC5308 on the right.

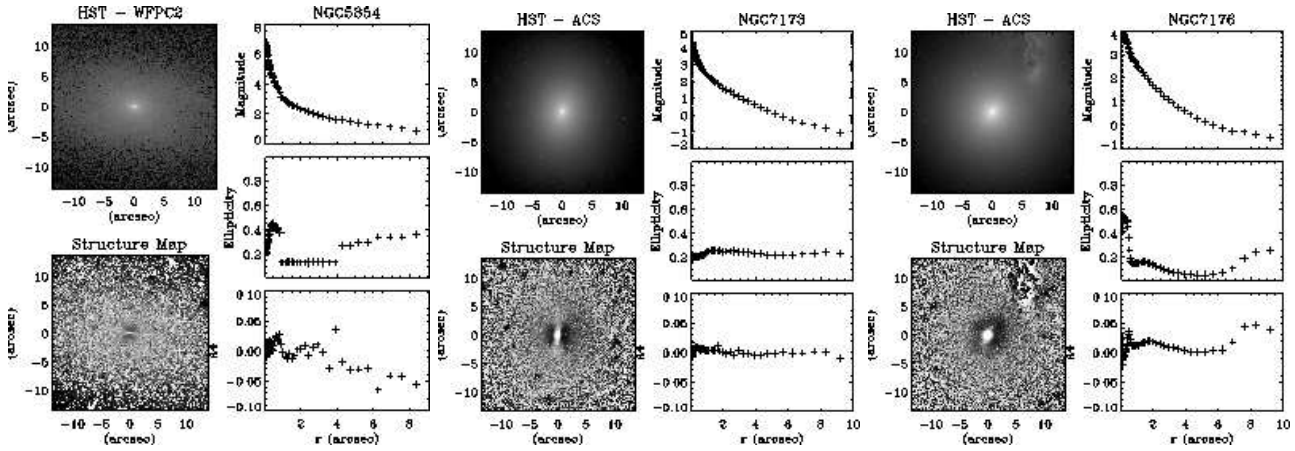

Figure A18. NGC5854 on the left, NGC7173 in the middle and NGC7176 on the right.

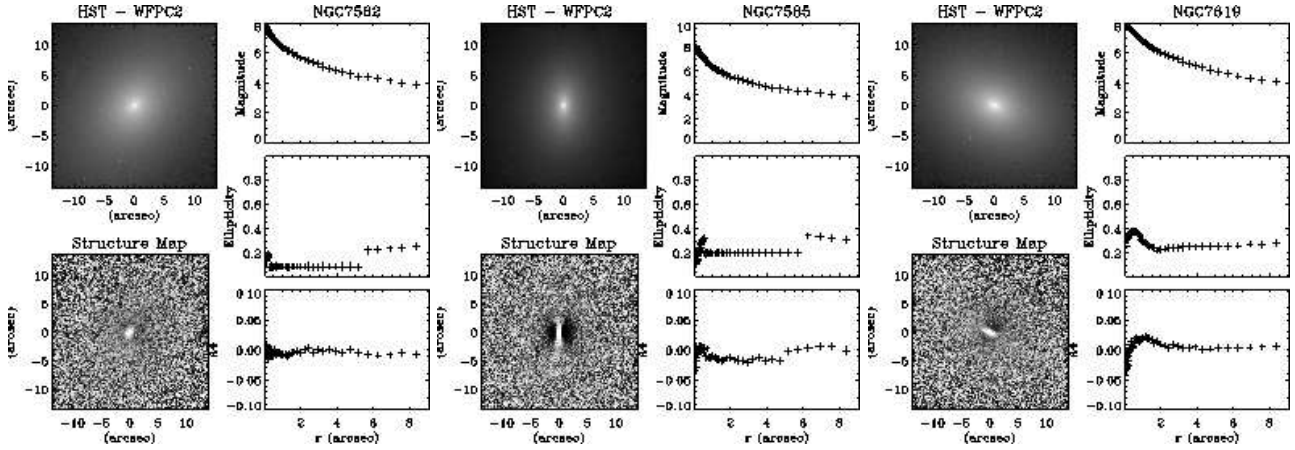

Figure A19. NGC7562 on the left, NGC7585 in the middle and NGC7619 on the right.

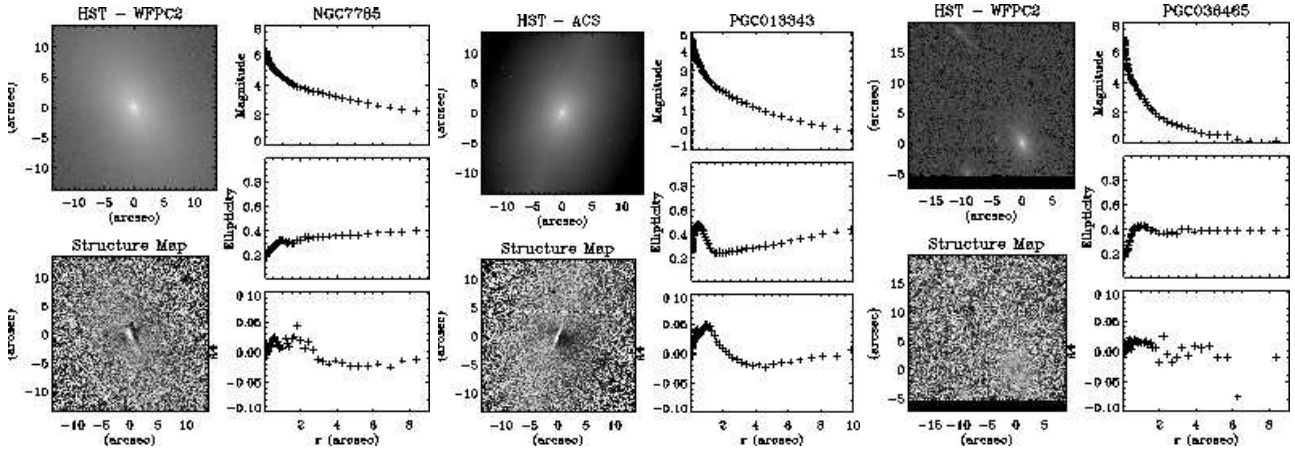

Figure A20. NGC7785 on the left, PGC013343 in the middle and PGC036465 on the right.

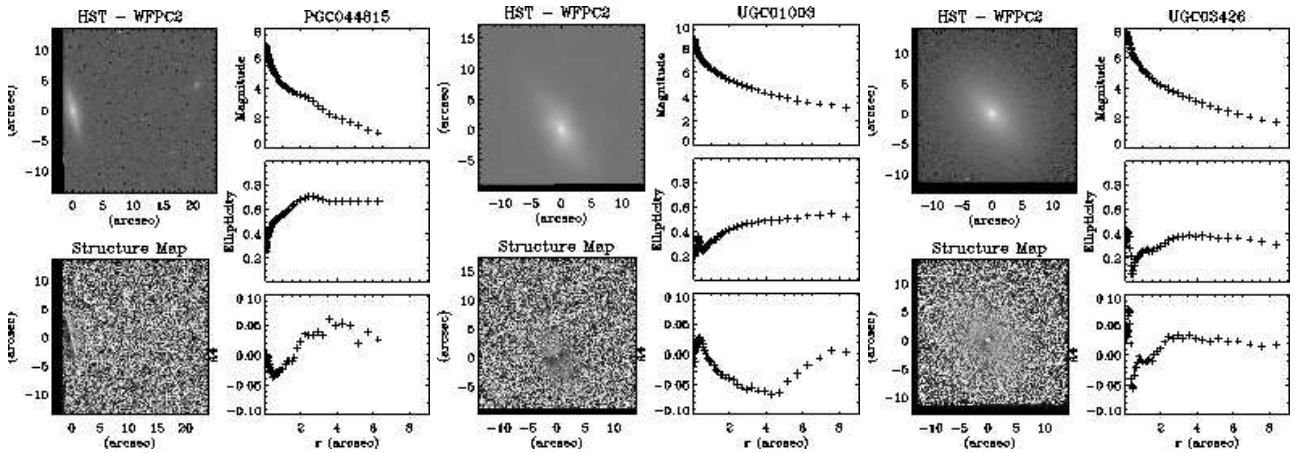

Figure A21. PGC044815 on the left, UGC01003 in the middle and UGC03426 on the right.

A3 Disk Decomposition

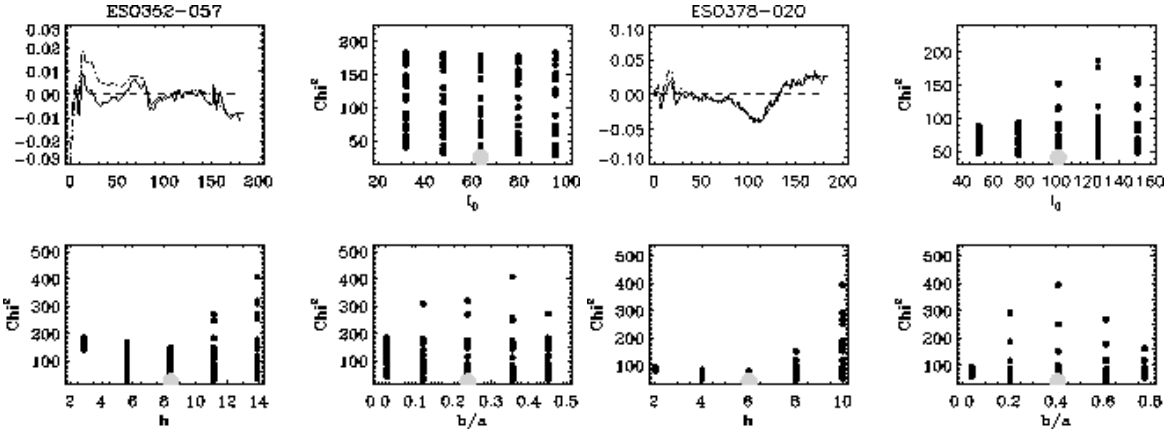

Figure A22. Scorza and Bender decomposition of ESO352-057 on the left and on the right.

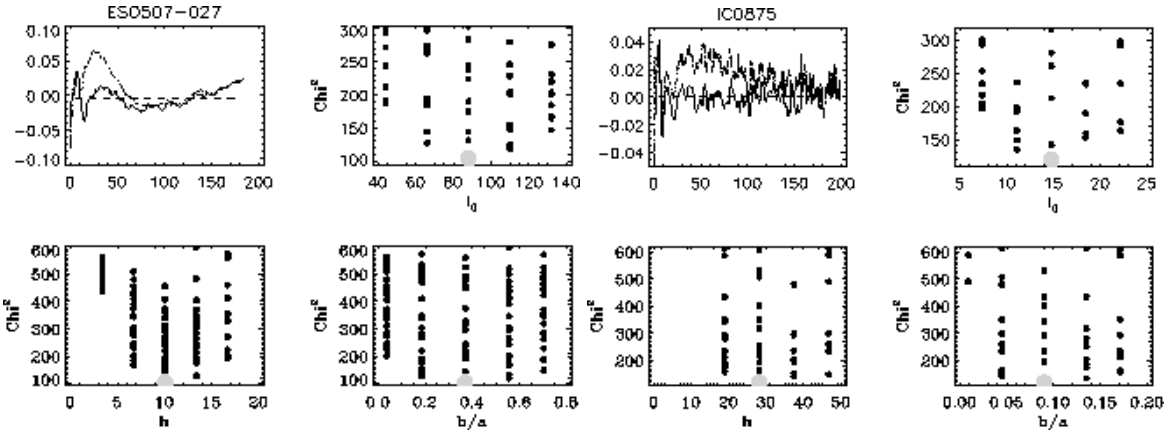

Figure A23. Scorza and Bender decomposition of ESO507-027 on the left and IC0875 on the right.

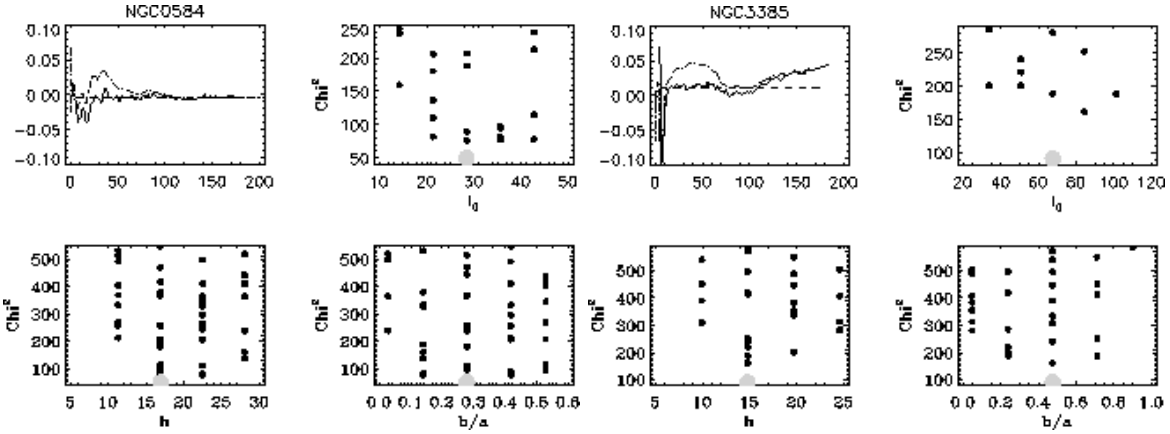

Figure A24. Scorza and Bender decomposition of NGC0584 on the left and NGC3385 on the right.

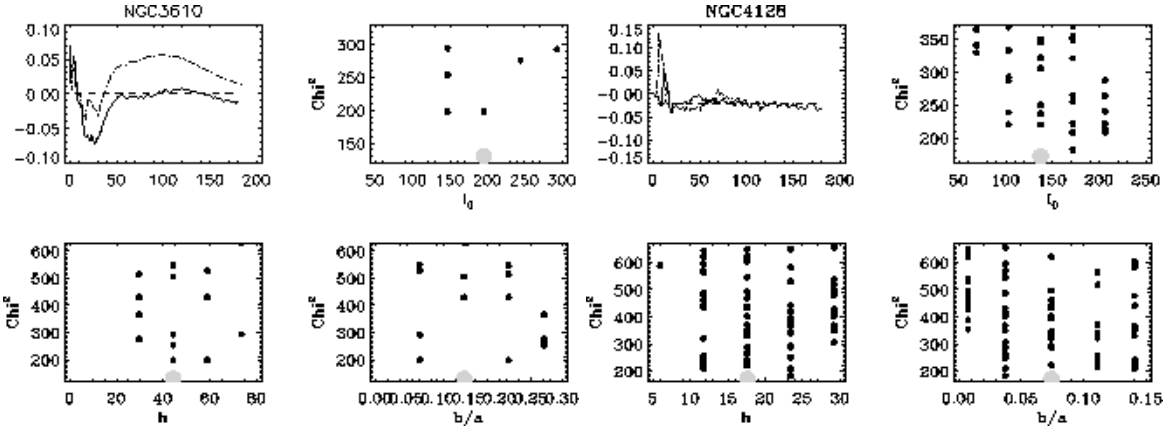

Figure A25. Scorza and Bender decomposition of NGC3610 on the left and NGC4128 on the right.

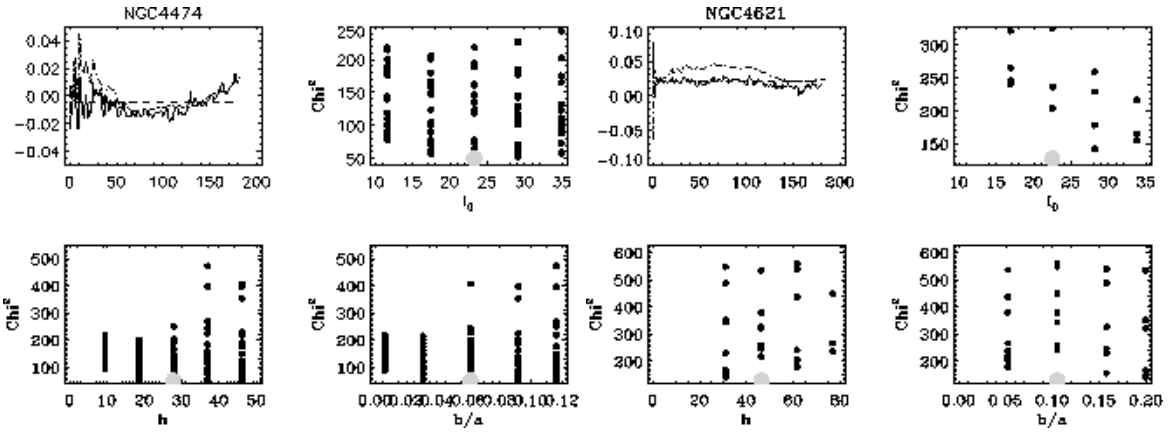

Figure A26. Scorza and Bender decomposition of NGC4474 on the left and NGC4621 on the right.

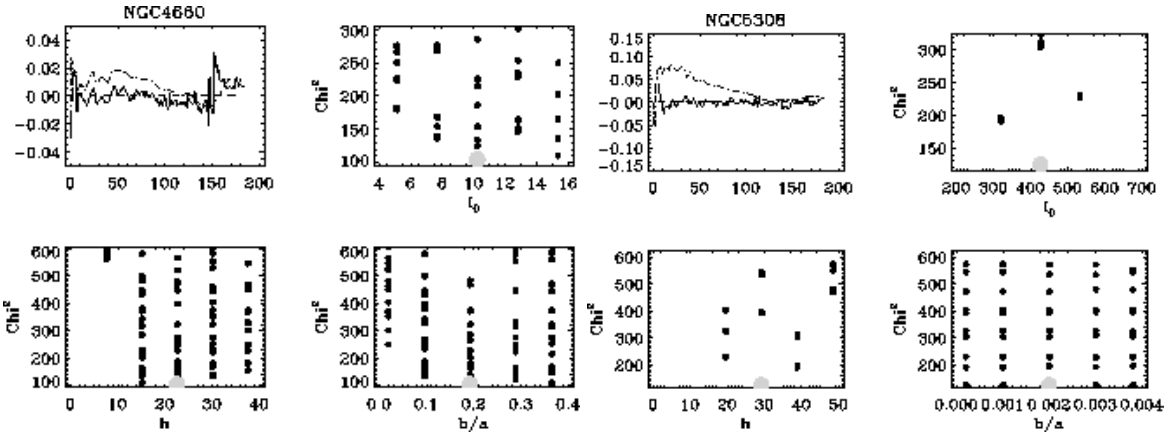

Figure A27. Scorza and Bender decomposition of NGC4660 on the left and NGC5308 on the right.